JOURNAL OF GEOPHYSICAL RESEARCH, VOL. 95, NO. B4, PAGES 4909–4923, APRIL 10, 1990

A Finite Amplitude Necking Model of Rifting in Brittle Lithosphere

JIAN LIN

Department of Geology and Geophysics, Woods Hole Oceanographic Institution, Woods Hole, Massachusetts

E. M. PARMENTIER

Department of Geological Sciences, Brown University, Providence, Rhode Island

We formulate a mechanical model describing the formation of rifts as finite amplitude necking of an elastic-plastic layer overlying a fluid substrate. A perfectly plastic rheology is a continuum description of faulting in rift zones. Two important aspects of rift evolution are illustrated by this model: the evolution of the rift width as extension proceeds and the finite strain that occurs. A region at yield initially develops with a width determined by the thickness of the brittle layer, and the internal deformation within this yield zone is proportional to the topographic slope. As extension proceeds, the surface within the rift subsides, and the width of the subsiding yield zone decreases. At any stage of rifting, material in regions just outside the yield zone is deformed but no longer deforming. The width of these deformed regions increases with increasing extension. Vertical forces due to the mass deficit of the rift depression will flex the elastic layer outside the yield zone, creating flanking uplifts. The external force required to maintain active rifting increases with the amount of lithospheric stretching, indicating that rifting is a quasi-static, stable process. Because the yield zone will revert to elastic behavior if the external force causing extension is removed, the model predicts that the rift depression and flanking uplifts will be preserved after extension stops. Our simple mechanical model demonstrates the inherent relationship among graben formation, lithospheric thinning, and rift shoulder uplift in rift zones.

Introduction

Rifting occurs where lithospheric extension is localized into a narrow zone. Rift zones have been identified both in continents and on ocean floor [*Burke*, 1978; *Ramberg and Neumann*, 1978; *Easton*, 1983; *Ramberg and Morgan*, 1984; *Rosendahl*, 1987]. Since continental rifts are a precursor of new ocean basins and mid-ocean ridge rifts occur where new oceanic crust is generated, understanding the evolution of rifts is of fundamental significance to the study of plate tectonics. Models which attempt to express our understanding of rifting mechanisms can be put into two major categories. The first category attributes rift structural and morphological characteristics to thermal processes in the lower lithosphere and asthenosphere. For example, rift shoulder uplift has been explained as the result of (1) lateral conduction of heat from extended to unextended lithosphere [e.g., *Cochran*, 1983]; (2) small-scale mantle convection driven by a lateral thermal gradient [e.g., *Buck*, 1986]; and (3) reequilibrium of a thermally stratified lithosphere in which the amount of extension varies with depth [e.g., *Royden and Keen*, 1980; *Keen*, 1985, 1987]. These models are concerned primarily with the thermal and mechanical behavior of the lower lithosphere and asthenosphere which deform in ductile (viscous) flow at high temperatures rather than brittle deformation of shallow lithosphere.

The second category of models investigate explicitly the deformation of brittle lithosphere in rift zones, especially those at the initiation stage. *Vening Meinesz* [1950] first suggested that a rift forms in an extending elastic lithosphere which fails by normal faulting. He argued that when an initial normal fault causes elastic flexure in a brittle lithosphere, a second normal fault will form where the flexural stresses are maximum. The initial and secondary normal faults thus comprise the boundary of a sinking rift graben. *Bott* [1976] and *Bott and Mithen* [1983] modified Vening Meinesz's model to include a ductile layer in the lower crust. In the modified model, while the brittle upper crust is stretched by normal faulting and graben subsidence, the ductile lower crust flows horizontally beneath the subsiding graben. These models, while attractive for their simplicity, cannot describe the extensive faulting and crustal thinning commonly observed in rift zones.

Deformation of brittle lithosphere in rift zones has also been treated as necking of a strong layer overlying a weaker substrate. *Artemjev and Artyushkov* [1971] qualitatively considered rifting as necking of a ductile crust which is mechanically strong near the surface and weaker at depth. They proposed that a perturbation in crustal thickness could induce nonuniform extension, which localizes stresses and generates a narrow zone of normal faults in the strong upper crust. This hypothesis was further developed and tested by *Zuber and Parmentier* [1986] and *Parmentier* [1987], who modeled lithosphere as a perfectly plastic layer, a continuum description of deformation on many faults. *Zuber and Parmentier* [1986] found that an initial perturbation in lithospheric thickness will amplify under extension. When this occurs, extension in the lithosphere will concentrate into a zone with a width comparable to the dominant wavelength, which depends only on lithospheric thickness and rheology. These necking instability models, however, are based on the assumption of small deformation amplitude and are not applicable to later stages of rifting when large finite strains have developed. In particular, since the analysis assumes a uniform state of horizontal extension

Paper number 89JB03059.
0148-0227/90/89JB-03059$05.00

onto which small-amplitude perturbations are superimposed, extensional deformation is not confined to a narrow zone within the rift [*Parmentier et al.*, 1987].

In this paper, we formulate a finite amplitude necking model of rifting in brittle lithosphere overlying ductile (viscous) substrate. Brittle failure and lithospheric extension are localized in a plastic yield zone beneath the rift basin. We demonstrate that the formation of such a region of necking makes it possible to explain lithospheric thinning, graben subsidence and rift shoulder uplifts in a self-consistent fashion. In the following sections we will examine the major characteristics of the plastic zone, its interaction with adjacent undeforming brittle lithosphere, and its control on rift evolution.

Model Mechanics

Studies of the rheology of the continental lithosphere [e.g., *Goetze and Evans*, 1979; *Brace and Kohlstedt*, 1980; *Kirby*, 1983] suggest a strong variation of strength with depth. Brittle deformation occurs in the upper crust, where lithospheric strength is controlled by frictional sliding on faults and the mode of faulting [*Byerlee*, 1968]. At greater depths, dislocation creep, which is chiefly a function of strain rate and temperature, is the dominant deformation mechanism. We idealize lithosphere as a brittle layer with thickness H and density ρ_l overlying a fluid with density ρ_a (Figure 1). This brittle layer represents the upper 12-15 km of a prerift continental crust or the upper few kilometers of oceanic lithosphere at a mid-ocean ridge. In general, stresses associated with ductile deformation in the lower continental crust and oceanic upper mantle depend on the width of the necking region and the rate of lithospheric extension. Viscous stresses associated with ductile mantle flow can influence greatly the short-term (100-200 years) postseismic relaxation of crustal earthquakes [*Rundle*, 1982; *Savage and Gu*, 1985] but should have a second order effect on long-term (~1 m.y.) rift basin-scale deformation [e.g., *Phipps Morgan et al.*, 1987; *Lin and Parmentier*, 1989]. Ductile (viscous) flow of the crust and mantle along with the resulting temperature variations could be treated by combining various ductile lithospheric stretching models [e.g., *Keen*, 1985, 1987] with our present analysis for necking in a strong brittle lithospheric layer. For simplicity, we treat the ductile lower lithosphere beneath continental rifts and the asthenosphere beneath oceanic rifts as inviscid fluids.

Lithospheric Faulting and Perfect Plastic Flow

In an extensively faulted media, if the characteristic spacing between faults in the media is much smaller than the size of the deforming region, we can approximate the motion on faults by perfect plastic flow. Closely spaced fractures and faults occur in many continental and oceanic rifts. In the Rhine graben, for example, the rift graben is framed by two inward facing master fault zones 40 km apart, while the rift valley itself is broken into internal tilted blocks by many sets of secondary normal faults. The characteristic distance between these secondary normal faults is only 1 km [*Illies*, 1972], far smaller than the 40 km width of the rift valley. Since we are concerned primarily with the overall characteristics of rifting instead of the specific motion on individual faults, perfect plastic flow is an acceptable approximation to motion on faults. Based on this same rationale, perfect plasticity has also been applied to describe deformation in mountain belts and accretionary wedges [*Elliott*, 1976; *Chapple*, 1978; *Davis et al.*, 1983].

In our model, the mechanical behavior of a rifted brittle lithosphere is characterized by a plastic yield zone embedded

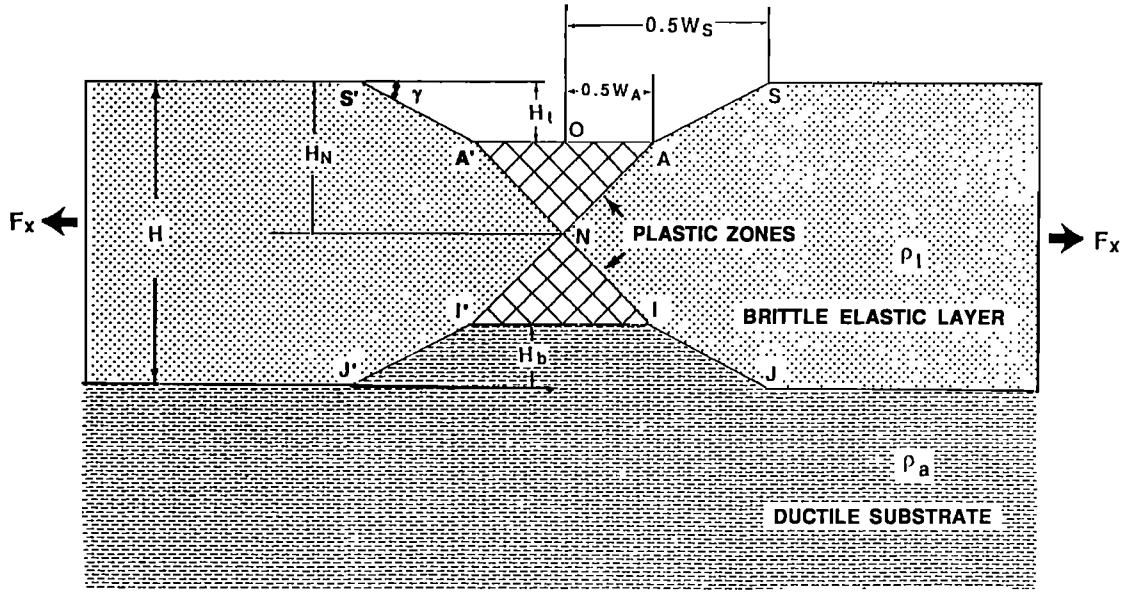

Fig. 1. A model of rift zone and definition of geometric parameters. Rheological stratum of rifts is modeled as a brittle layer overlying a ductile substrate. The rift zone is characterized as a plastic yield zone embedded in an otherwise elastic lithsophere. In general, it is possible for an upper plastic yield zone and a lower plastic zone to coexist, with N as the connecting point. The relative sizes of the two plastic zones is described by the location of connecting point N. H_l is the rift basin depth, and H_b is the relif on the lower plastic zone. W_A is the width of the active rift valley, and W_S is the distance between rift shoulders.

in an otherwise elastic lithosphere (Figure 1). This model does not describe the initiation stages of rifting but assumes that many faults defining the yield zone are already present. In general, plastic solutions allow the coexistence of an upper plastic zone (area A'NA in Figure 1) and a lower plastic zone (area I'NI in Figure 1). The location of point N is not determined by mechanical equilibrium conditions alone but by energy considerations, as will be discussed later. The important geometric parameters include the depth of rift basin, H_t; the relief on the bottom of the plastic layer, H_b; the width of rift valley, W_A; and the distance between the flanks of rift shoulders, W_S. Since the mechanical properties of the lithospheric material are different inside and outside the plastic zone, different mathematical formulations are needed, accordingly. Solutions will be developed first for the plastic zone and then for the elastic plates.

Perfect plasticity is characterized by the existence of a mechanical yield point beyond which permanent strain appears. While most metals at low temperatures obey the pressure-independent von Mises failure criterion, soils and sands commonly exhibit pressure-dependent yielding behavior in accord with the Coulomb (frictional-type) criterion. Since the strength of the brittle lithosphere is controlled by frictional properties of rocks [e.g., *Brace and Kohlstedt*, 1980], the Coulomb criterion is more appropriate for crustal material. Although the two failure criteria predict deformation patterns which are different in detail, the fundamental features are the same. To maintain both generality and simplicity, the mathematical formulations that we give are applicable to both von Mises and Coulomb materials, while the calculated examples employ the simpler von Mises material.

The yield stress of a von Mises material is equal to a pressure-independent parameter k, whose value depends mainly on the material type. In this type of material, brittle failure occurs along planes on which the maximum resolved shear stress $\tau = k$. The von Mises criterion can be written as

$$(\sigma_3-\sigma_1)^2/4 = (\sigma_x-\sigma_y)^2/4 + \tau_{xy}^2 = k^2 \qquad (1)$$

where σ_1 and σ_3 are the minimum and maximum tensile stresses, σ_x, σ_y, and τ_{xy} are the stress components in a x-y coordinate system (as defined in Figure 2).

The yield stress of a Coulomb (frictional type) material is pressure-dependent. The frictional sliding on a typical failure plane is governed by $|\tau| = C_o + (-\sigma_n)\tan\phi$, where C_o and ϕ are the cohesion and angle of friction of the material and σ_n is the normal stress across the failure plane (Figure 3*a*). In an x-y coordinate system, this criterion is expressed as

$$(\sigma_x-\sigma_y)^2/4 + \tau_{xy}^2 = [(\sigma_x+\sigma_y)\sin^2\phi + C_o]^2 \qquad (2)$$

The von Mises criterion can be regarded as a special case of the Coulomb criterion, when $C_o = k$ and $\phi = 0$.

Stress Field in Plastic Yield Zone

The magnitude of the plastic flow strains within the central plastic zone is far greater than the elastic strains in the adjacent lithospheric plates. When calculating the deformation of the plastic zone, these elastic lithospheric plates can be regarded as rigid and the changes in the plastic-elastic boundaries due to elastic deformation can be neglected [*Hill*, 1950]. Therefore the deformation of the elastic plates is considered only when we later calculate the uplift of rift shoulders due to the formation of a rift basin.

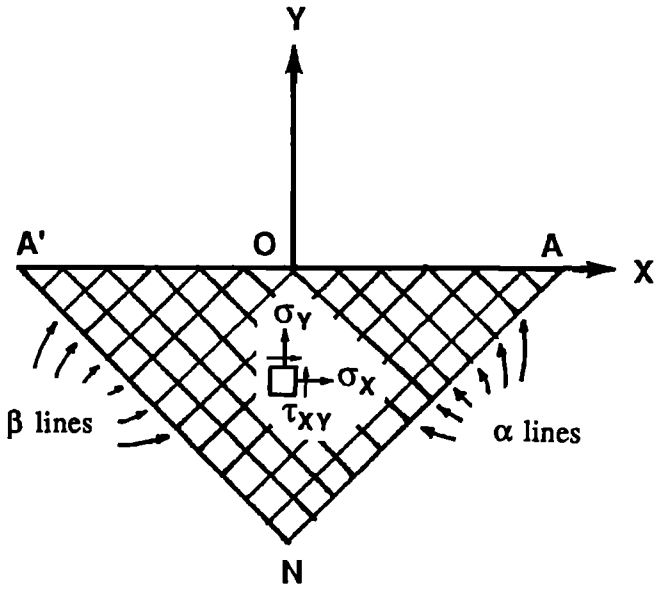

Fig. 2. The x-y coordinate system and plastic characteristic lines in a rift yield zone. The inclined lines are lines of stress or velocity characteristics. For a von Mises material, the stress and velocity lines coincide. For a Coulomb-type material, however, stress characteristic lines have different inclination angle from velocity characteristic lines. The parameters α and β represent conjugate characteristic lines.

A complete description of flow within the plastic zones requires the determination of stress and velocity at each point. For plane strain deformation there are five unknowns: three components of stresses σ_x, σ_y, τ_{xy} and two components of velocity u_x, u_y. Five independent equations are therefore necessary to solve for both stresses and velocities.

The yield criteria, equation (1) or (2), provide one of the basic equations for determining stress field. The other two basic equations required for the determination of stresses come from the consideration that stresses must be at equilibrium at each point:

$$\partial\sigma_x/\partial x + \partial\tau_{xy}/\partial y = 0 \qquad (3a)$$

$$\partial\sigma_y/\partial y + \partial\tau_{xy}/\partial x = -\rho_1 g \qquad (3b)$$

where g is the acceleration of gravity.

Although equations (1), (3*a*) and (3*b*) are the fundamental equations in the plastic problem, the mathematical nature of these equations is difficult to understand without further derivations. We therefore express the stresses as functions of two new parameters σ and θ [*Sokolovskii*, 1965], where $\sigma = -p + C_o/\tan\phi$, p is an average stress, and θ represents the angle between the maximum principal stress direction and the x- axis (Figure 3*b*),

$$\sigma_x = \sigma\,(1 + \sin\phi\cos2\theta) - C_o/\tan\phi \qquad (4a)$$

$$\sigma_y = \sigma\,(1 - \sin\phi\cos2\theta) - C_o/\tan\phi \qquad (4b)$$

$$\tau_{xy} = \sigma\sin\phi\sin2\theta \qquad (4c)$$

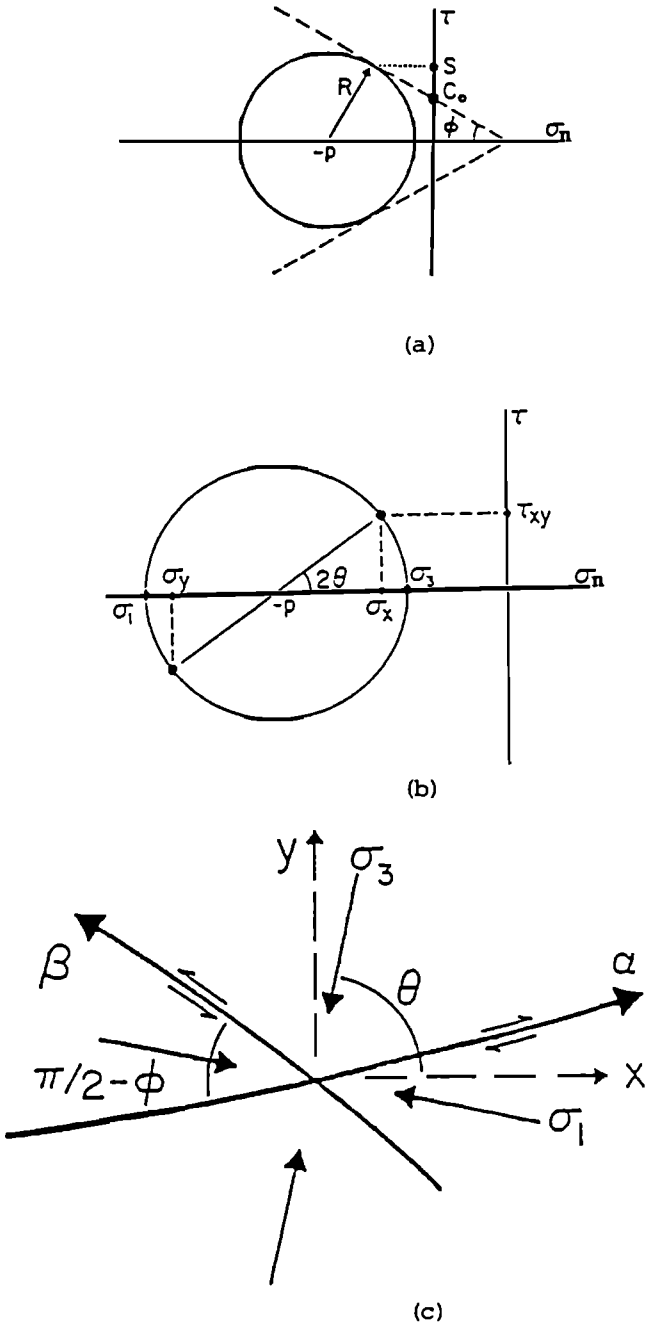

Fig. 3. (*a*) Failure criteria of frictional or Coulomb-type (pressure dependent) material. At any point in space the Mohr failure envelope consists of two straight lines with slopes of $\pm\tan\phi$ (where ϕ is the angle of internal friction) and intercepts of $\pm C_0$. (*b*) Stress convention. Compressive stress is negative, with $\sigma_3 > \sigma_1$ algebraically (σ_3 is the least compressive stress). (*c*) Relation of stress characteristic lines to principal stresses. Stress characteristic lines are designated either α lines or β lines depending upon whether they have a right-handed or left-handed sense of shear across them, respectively. The angle formed by the stress characteristic lines is $\pi/2-\phi$; θ is the counterclockwise angle from the x direction to the σ_3 direction.

In this functional transformation, we have assumed that the material is at yield so that the failure criteria (equation (2)) can be employed to reduce the three unknowns σ_x, σ_y, and τ_{xy} to only two unknowns σ and θ. Substitution of (4) into (3) results in a quasi-linear system of first order partial differential equation in $\sigma(x,y)$ and $\theta(x,y)$:

$$(1 + \sin\phi\cos2\theta)\,\partial\sigma/\partial x + \sin\phi\sin2\theta\,\partial\sigma/\partial y - 2\sigma\sin\phi\,(\sin2\theta\,\partial\theta/\partial x - \cos2\theta\,\partial\theta/\partial y) = 0 \quad (5a)$$

$$\sin\phi\sin2\theta\,\partial\sigma/\partial x + (1 - \sin\phi\cos2\theta)\,\partial\sigma/\partial y + 2\sigma\sin\phi\,(\cos2\theta\,\partial\theta/\partial x + \sin2\theta\,\partial\theta/\partial y) = -\rho_1 g \quad (5b)$$

This system of equations is hyperbolic and can therefore be solved by the method of characteristics [*Sokolovskii*, 1965, p.29].

The solutions to equations (5*a*) and (5*b*) are described in terms of stress characteristic lines [*Hill*, 1950]. In von Mises material, the stress characteristic lines (also called slip lines) coincide with directions of maximum resolved shear stress. Slip lines with a right-handed or left-handed sense of shear are called α lines or β lines, respectively (Figure 2). In an x,y coordinate system, they form a right-handed set of curvilinear coordinate axes where the algebraically largest (least compressive) principal stress lies in the first and third quadrants (Figure 3*c*).

Except for a few geometrically simple cases for which full analytical solutions can be obtained, the hyperbolic equations (5) must be solved numerically. *Sokolovskii* [1965] shows that these equations are reducible to a simpler set of equations of characteristics :

$$dy = dx\tan(\theta \mp \varepsilon) \quad (6a)$$

$$d\sigma = 2\sigma\tan\phi\,d\theta \pm \rho_1 g/\cos\phi\,(\mp\sin\phi\,dx + \cos\phi\,dy) \quad (6b)$$

where $\varepsilon = \pi/4 - \phi/2$. The first equation of equation (6*a*) (with minus sign in front of ε) describes the geometry of α lines, and the first equation of equation (6*b*) (with plus sign in front of $\rho_1 g/\cos\phi$) describes the relationship between σ and θ along the same α lines. Similarly, the second equations of equations (6*a*) and (6*b*) apply to the β lines. From these basic equations, a slip line field can be constructed numerically using finite difference approximations.

The stress boundary conditions are known only at the upper and lower surfaces of the plastic yield zone. At the upper surface, stress free conditions apply, namely,

$$\sigma_n = 0 \quad (7a)$$

$$\sigma_s = 0 \quad (7b)$$

At the lower surface (the interface between the plastic zone and ductile substrate), the shear stress is zero due to the assumed inviscid ductile substrate, and the hydrostatic normal stress is given by

$$\sigma_n = -\rho_1 g H + \rho_a g H_b \quad (8a)$$

$$\sigma_s = 0 \quad (8b)$$

where H_b is the vertical displacement of the lower surface from its initial height. Since the stress boundary conditions in equations (7) and (8) do not involve velocities, the stress field in the plastic zone is determined independent of velocity field [*Hill*, 1950]. The procedure to determine numerically the slip line field in the plastic zone is given in Appendix A.

Velocity Field in Plastic Yield Zone

Once the stress field has been determined, a velocity field can be calculated given sufficient velocity boundary conditions. To determine velocity boundary conditions, we consider that the two elastic lithospheric plates move away from the center with a speed u_0.

For an incompressible material, the divergence of the velocity field must vanish:

$$\partial u_x/\partial x + \partial u_y/\partial y = 0 \quad (9)$$

A material property of an isotropic plastic material is that the principal axes of stress and strain rate coincide [*Hill*, 1950]:

$$2\tau_{xy}/(\sigma_x-\sigma_y) = (\partial u_y/\partial x + \partial u_x/\partial y)/(\partial u_x/\partial x - \partial u_y/\partial y) \quad (10)$$

Substitution of (6) into (10) gives

$$(\partial u_x/\partial y + \partial u_y/\partial x)\ \tan 2\theta + (\partial u_x/\partial x - \partial u_y/\partial y) = 0 \quad (11)$$

Equations (9) and (11) form a system of hyperbolic equations for velocity field, whose characteristic lines coincide with the stress characteristic lines (slip lines) for von Mises material only. Similar to the stress equations, these velocity equations are reducible to the equations of characteristics [*Salencon*, 1974]:

$$du_\alpha - u_\alpha \tan\phi\, d(\theta - \phi/2) - u_\beta/\cos\phi\, d(\theta - \phi/2) = 0 \quad \text{along an } \alpha \text{ line} \quad (12a)$$

$$du_\beta + u_\alpha/\cos\phi\, d(\theta + \phi/2) + u_\beta \tan\phi\, d(\theta + \phi/2) = 0 \quad \text{along a } \beta \text{ line} \quad (12b)$$

From (12) it follows that velocity characteristic lines are lines of zero incremental extension and that instantaneous discontinuities in the velocity field can occur only in the tangential planes across these lines. Finite-difference equivalences of equation (12) are used to determine numerically the velocity field in the plastic zone (see Appendix A).

Results

The calculated geometry of plastic yield zones with a prescribed rift valley topographic slope is shown in Figure 4*a* for a von Mises material. The corresponding velocity field in the plastic zones in Figure 4*b* shows several velocity discontinuity planes in the plastic zones. The most prominent velocity discontinuity is along the boundary between the plastic zones and the elastic lithospheric plates (line ABCN and line A'B'C'N). Secondary velocity discontinuities occur along several planes inside the plastic zones (e.g., line OB and line OC). The magnitude of the secondary velocity discontinuities is proportional to the topographic slope.

If the top and bottom of the plastic zones are initially flat, deformation within the these zones is considerably simpler. The evolution of such plastic zones is shown in Figure 5 for a rift with symmetric upper and lower plastic zones. Both the stress patterns (left) and instantaneous velocity fields (right) are illustrated for different amounts of total surface extension ΔL. At $\Delta L = 0$, the upper and lower boundaries of the yield zone have not deformed, and both the α and β lines are inclined to the horizontal surfaces at angle $\pi/4$. The velocity field at $\Delta L = 0$ indicates four blocks of distinctive instantaneous motion (Figure 5*b*).

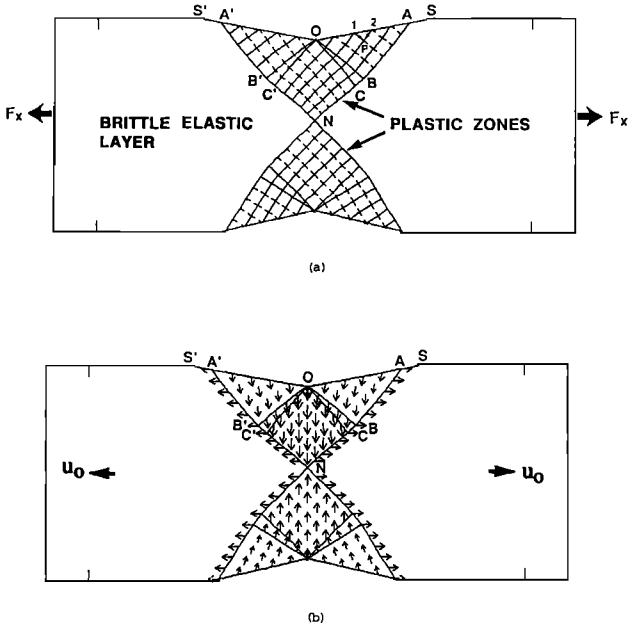

Fig. 4. (*a*) Calculated plastic zone geometry and stress characteristic lines for a rift zone with inclined topography. The solid lines are α lines and dashed lines, are β lines. (*b*) Calculated velocity field corresponding to stress solutions of Figure 4*a*. Note that major velocity discontinuities occur at the boundary between the plastic zone and elastic plates, while secondary discontinuities occur along several planes inside the plastic zone.

Simple Shear Discontinuities Framing Plastic Yield Zones

As the two elastic lithospheric plates move apart at a velocity u_0, the material in the upper plastic zone moves downward at speed u_0, while the material in the lower part moves upward at the same speed. The change of the rift zone geometry can be readily observed by comparison of the rift configuration at $\Delta L = 0$ and that at $\Delta L = 0.2$ H (Figure 5). At $\Delta L = 0.2$ H, both the upper and lower plastic zones become smaller from the initial configulations, but they are still connected at the same point. Notice that the material within the narrow, shaded bands at $\Delta L = 0.2$ H was within the plastic zone at $\Delta L = 0$ but now has become a part of the elastic plates. A finite amplitude simple shear develops discontinuously across the slip lines defining the edge of the yield zone. In the example illustrated in Figure 5, point N is assumed fixed, so are the location of the slip lines with simple shear. Clay experiments illustrated in Figure 6 [*Cloos*, 1968] show similar velocity fields to those in Figure 5*b* with narrow lines across which velocity vectors change direction dramatically. Similar lines of velocity discotinuities have also been observed in sandbox experiments [*Horsfield*, 1980].

According to mechanical characteristics and deformation history, a rifted brittle lithosphere can be divided into three subregions (Figure 5*a*). Region 1 is within the plastic yield zone. The upper plastic zone is the rift graben. The size of

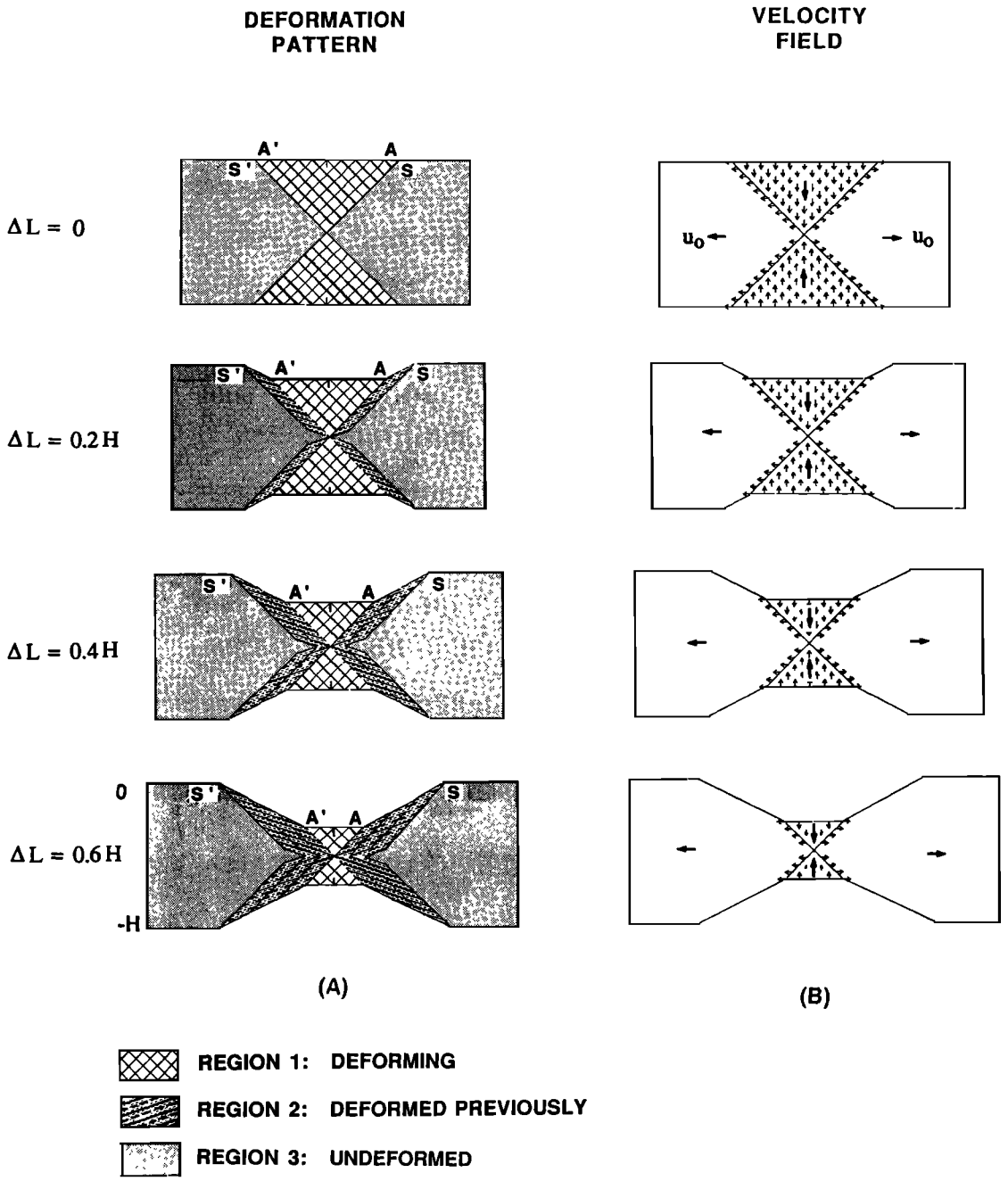

Fig. 5. Evolution of rift geometry in absence of regional isostatic compensation. (*a*) Plastic zone geometry at various stages of rifting. There are three regions with different deformation characteristics and history. Region 1 is within the plastic zone. The inclined lines in the plastic zones are the lines of velocity characteristics. Internal deformation can occur in this region. In region 2 the material has previously deformed but is presently a part of the elastic plate. Region 3 is the undeformed part of the brittle lithosphere. (*b*) Velocity fields at various stages of rifting. In general, the velocity fields in the plastic zones are not uniform. The example shown is for a special case when the top and bottom boundaries of the plastic zones are flat. Note that velocities are discontinuous at the boundaries between the plastic zones and the elastic plates.

this region decreases as rifting progresses. If the topography of rift valley is not flat, internal deformation will occur within this region and velocity will not be uniform as in this simple example. The inclined lines are velocity characteristic lines. Region 2 is presently part of the rigid lithospheric plate, although it deformed in the past by plastic flow. The size of this region increases as rifting progresses. Region 3 is undeformed material. In continental rifts, major active normal faults were found to be within narrow zones framing rift grabens [*Illies*, 1972; *Ebinger et al.*, 1984; *Shudofsky*, 1985; *Rosendahl*, 1987]. It was also found that all of the minor active faults occur only within the rift graben, and the surface scarps beyond the major boundary fault system correspond to inactive

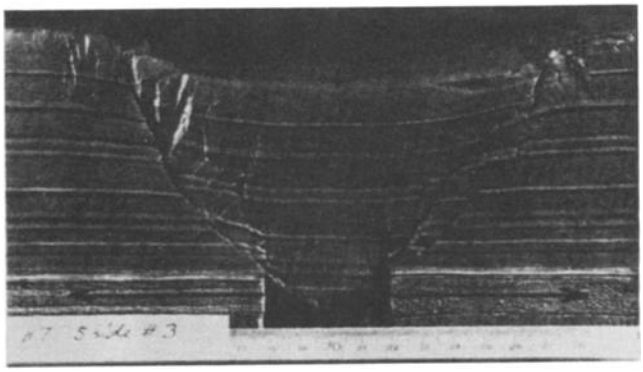

a

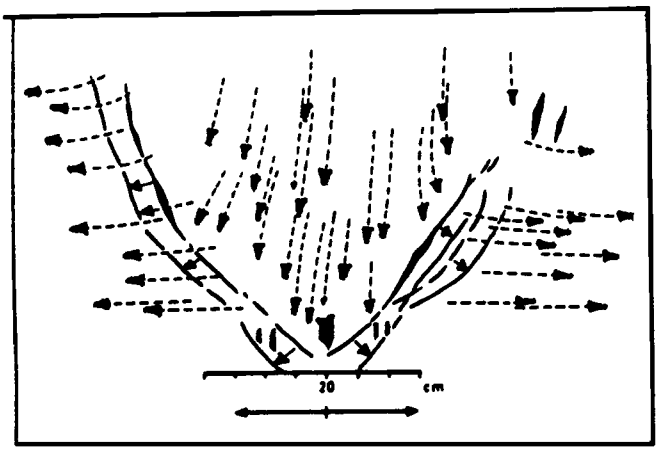

b

Fig. 6. (*a*) Graben formation in clay experiment, in which clay graben slid down between blocks after symmetrical pull [*Cloos*, 1968]. In this particular experiment, displacement along the graben boundary is 20 mm on right side and 22 mm on left side. Scale in cm. (*b*) Migration of reference points during deformation [*Cloos*, 1968] as traced from successive photographs. Note the close similarity between this velocity field and the predicted velocity field in the upper plastic zone in Figure 5*b*.

faults [*Gibbs*, 1984; *Ebinger et al.*, 1987]. The deformation pattern of our model is generally in agreement with these observations.

The predicted surface slope γ (Figure 1) of the deformed region (in absence of erosion) is given by

$$\tan \gamma = 0.5 \qquad (13a)$$

or

$$\gamma = \tan^{-1}(0.5) \approx 27^{o} \qquad (13b)$$

This slope is inherently determined by the initial surface slope (0^{o}) and the inclination of the shear slip lines framing plastic zones (45^{o}) and is independent of the separation velocity of the two elastic plates.

Although the stress and velocity lines coincide for the von Mises material as in the example of Figure 5, they might not in other cases. For the same boundary conditions, if a Coulomb-type material with 30^{o} of angle of internal friction was considered instead, the stress lines would incline 60^{o} to the flat surface (equation (6*a*)) while velocity lines remain at 45^{o} inclination. Since the finite strain in plastic zones is determined by the incremental accumulation of displacements, it is the velocity characteristic lines, not the stress characteristic lines, which control the evolving geometry of a rift zone. In addition, which of the velocity characteristic lines is active is determined by specific velocity boundary conditions. It is therefore incorrect to interpret stress characteristic lines as faults or even as planes of potential faults, as was suggested in the earlier model of *Hafner* [1951].

Although the example illustrated in Figure 5 is for a special case when the upper and lower plastic zones are symmetric, the conclusions hold for other rifts with asymmetric upper and lower plastic zones. See Figure 8 for another special example in which there is only an upper plastic zone.

Thinning of Lithosphere and Shrinking of Plastic Zone

As rifting progresses, the plastic zones become narrower. This reduces lithospheric thickness beneath the rift valley and narrows the width of rift valley (Figure 5). The geometric variables of the rift valley and plastic zones can be expressed in terms of the layer thickness H, the thickness of the upper plastic zone H_N, and the total amount of surface extension ΔL:

$$H_t = (1/2)\,\Delta L \quad \text{(if the upper plastic zone is present)} \qquad (14a)$$

$$H_b = (1/2)\,\Delta L \quad \text{(if the lower plastic zone is present)} \qquad (14b)$$

$$\Delta H = H_t + H_b \qquad (14c)$$

$$W_A = 2H_N - \Delta L \qquad (14d)$$

$$W_S = 2H_N + \Delta L \qquad (14e)$$

where ΔH is the amount of lithospheric thinning due to rifting. We note that while the width of rift valley W_A narrows, the distance between the flanks of rift shoulder, W_S, increases. The difference between these two widths, therefore, reflects the amount of rift extension. More examples are shown in Figure 10.

Even for rift zones at their early stages of rifting (such as the Lake Tanganyika of the East African Rift), stratigraphic records on sedimentary basins indicate narrowing of active deformation zones [*Ebinger et al.*, 1984, 1987; *Rosendahl*, 1987]. Other examples of narrowing of extension zone can be found in the Rhine graben [*Villemin et al.*, 1986], the U.S. Atlantic passive margin [*Steckler and Watts*, 1982; *Kligfield et al.*, 1984], and the Baikal rift [*Zorin and Rogozhina*, 1978].

Discussion

Stress Distribution in Plastic Zones

It is easy to verify that the stress field in the upper plastic zone ($H_t < y < H_N$) is given by

$$\sigma_x = -\rho_1 g y + \rho_1 g H_t + 2k \qquad (15a)$$

$$\sigma_y = -\rho_1 g y + \rho_1 g H_t \qquad (15b)$$

$$\tau_{xy} = 0 \qquad (15c)$$

Similarly, in the lower plastic zone ($H_N < y < H\text{-}H_b$) the stress field is given by

$$\sigma_x = -\rho_l g y + (\rho_a - \rho_l) g H_b + 2k \quad (15d)$$

$$\sigma_y = -\rho_l g y + (\rho_a - \rho_l) g H_b \quad (15e)$$

$$\tau_{xy} = 0 \quad (15f)$$

For convenience, we define deviatoric stresses $\bar{\sigma}_x$, $\bar{\sigma}_y$, $\bar{\tau}_{xy}$ as the stresses in excess of the lithostatic overburden, namely, in the upper plastic zone,

$$\bar{\sigma}_x = \sigma_x + \rho_l g y = \rho_l g H_t + 2k \quad (16a)$$

$$\bar{\sigma}_y = \sigma_y + \rho_l g y = \rho_l g H_t \quad (16b)$$

$$\bar{\tau}_{xy} = \tau_{xy} = 0 \quad (16c)$$

Similarly, in the lower plastic zone,

$$\bar{\sigma}_x = \sigma_x + \rho_l g y = (\rho_a - \rho_l) g H_b + 2k \quad (16d)$$

$$\bar{\sigma}_y = \sigma_y + \rho_l g y = (\rho_a - \rho_l) g H_b \quad (16e)$$

$$\bar{\tau}_{xy} = \tau_{xy} = 0 \quad (16f)$$

Therefore, when the top and bottom boundaries of the plastic zones are flat and when the boundary stresses are uniform, the deviatoric stresses in the plastic zones are uniform. An example of the deviatoric stress solutions (equations (16)) are plotted in Figure 7 for a 10-km brittle lithosphere with a von Mises yield limit of 2k = 80 MPa, a value that corresponds to the average brittle strength of continental crust [*Brace and Kohlstedt*, 1980].

Minimum Work Solution

For the deformation of perfect plastic material the equilibrium equations alone do not always lead to unique stress and velocity fields. An example of this nonunique nature can be seen in Figure 1, where plastic solution permits point N at any level. The corresponding solutions satisfy all boundary conditions as well as the failure criterion. Therefore it is necessary to include supplementary mechanical considerations. A preferred solution is determined by energy considerations.

The rate of increase of gravitational potential U of plastic zones is given by

$$dU/dt = \int_v -\rho_l g u_y \, dxdy \quad (17a)$$

where u_y is the vertical velocity, and the integration should be performed over the entire plastic zones (areas A'NA and I'NI in Figure 1).

The rate of energy dissipation E by the plastic zones in resisting the shear strength of the lithospheric material can be evaluated by

$$dE/dt = \int_v (1/2)\,(\partial u_i/\partial x_j + \partial u_j/\partial x_i)\,\sigma_{ij} \, dxdy \quad (17b)$$

where u_i (i = 1, 2) are the x, y components of velocity field and σ_{ij} (i,j = 1, 2) are components of stress tensor.

The rate of work W performed on the plastic zones by the two adjacent elastic plates and the inviscid substrate is given by

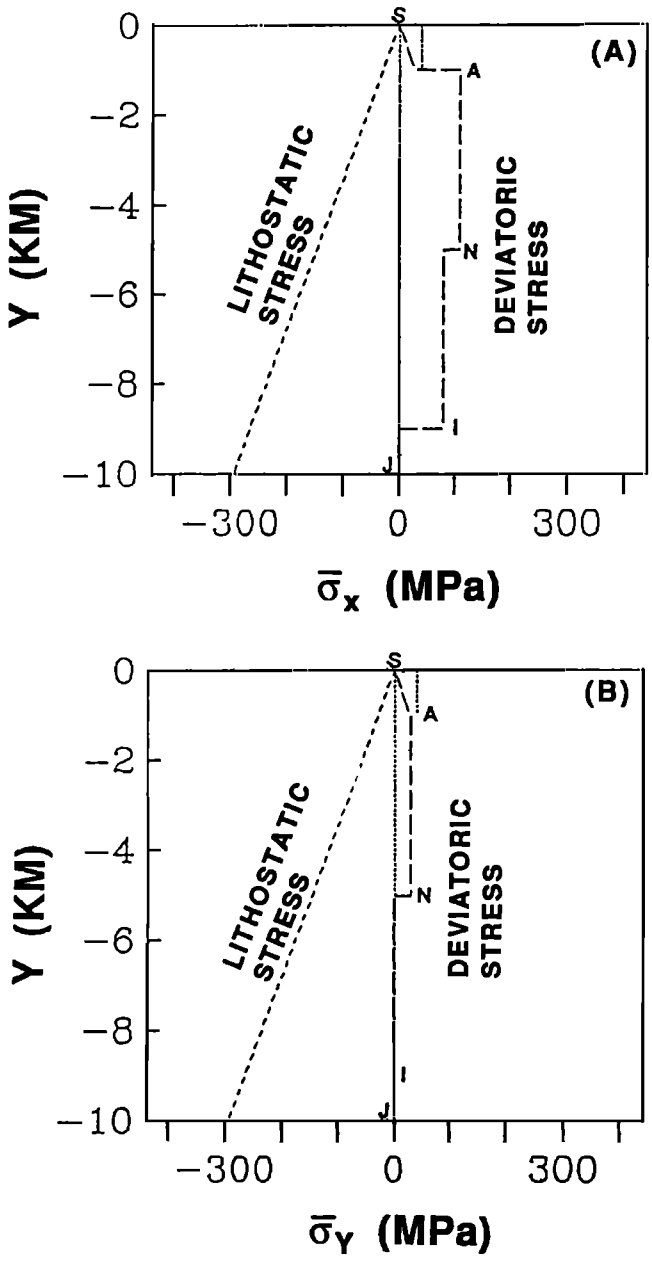

Fig. 7. Vertical distribution of deviatoric stresses along line SANIJ (Figure 1). (*a*) The long dashed line shows the horizontal deviatoric stress $\bar{\sigma}_x$ as a function of depth. Lithostatic stress is plotted by a short dashed line as a reference. (*b*) The long dashed line shows the vertical deviatoric stress $\bar{\sigma}_y$ as a function of depth. Again lithostatic stress is plotted by a short dashed line.

$$dW/dt = \int_{s=\partial v} u_i t_i \, ds \quad (17c)$$

where t_i (i = 1,2) are the normal and tangential components of traction forces on plastic zone boundary and u_i (i = 1,2) are the normal and tangential components of the velocity vector. The integration should be performed over the entire boundary of the plastic zones (lines A'A, AN, and NA and lines NI, II', and I'N in Figure 1).

We know that the work done by the forces transmitted through the elastic plates and by the substrate must equal energy dissipated in the plastic deformation plus the change in potential energy:

$$dW/dt = dE/dt + dU/dt \quad (18)$$

It is straightforward to evaluate the rate of increase of gravitational energy of plastic zones during rifting using equations (15) and (17*a*):

$$dU/dt = - u_o\rho_1 g\,[(H_N-H_t)^2 - (H-H_N-H_b)^2] \quad (19a)$$

Similarly, the rate of work performed by the two elastic plates and the inviscid substrate can be elavulated using equations (15) and (17*c*):

$$dW/dt = 2u_o k\,(H-H_t-H_b)$$

$$- u_o\rho_1 g\,[(H_N-H_t)^2 - (H-H_N-H_b)^2] \quad (19b)$$

To evaluate the rate of energy dissipation by plastic zones (equation (17*b*)), we note that velocity gradient is present only along the plastic zone boundaries (lines AN, A'N, NI, and NI' in Figure 1). The resultant tangential velocity component along these boundaries is $\sqrt{2}/2\ u_o$, and the resultant shear stress along these boundaries is k. The integration in equation (17*b*) is therefore replaced by the summation of stress work along lines AN, A'N, NI, NI' in Figure 1, which gives

$$dE/dt = 2u_o k\ (H-H_t-H_b) \quad (19c)$$

From the expressions of equations (19*a*), (19*b*) and (19*c*), it is obvious that the fundamental relationship of equation (18) is satisfied.

Examining the deformation history in Figure 5, we notice that the gravitational potential of the upper plastic zone is reduced during extension while that of the lower plastic zone is increased. The reduction rate of the gravitational potential is maximum when there is only an upper plastic zone (H=H_N in equation (19*a*)). We argue that this is the preferred mode of deformation in rifts since the rate of work required by the elastic plates and ductile substrate is minimumized (equation (19*b*)). In this preferred solution for rifting (Figure 8), the upper plastic zone collapses under its own weight; the gravitational potential released is converted into energy dissipation in plastic flow.

When a viscous substrate is considered, additional terms due to viscous stresses must be added to the boundary conditions of lower plastic zone (equation (8)), and the stress distribution in the plastic zones should be reevaluated. In Appendix B, we derive analytic solutions for the stress and velocity fields of a viscous half-space with a flat surface. We show that although the stress field in the viscous half-space is a function of the width of the lower plastic zone, the total rate of energy dissipation in resisting viscous flow does not depend on the geometry of the lower plastic zone. Therefore, the conclusions we have reached for inviscid substrate hold valid for viscous substrate as well.

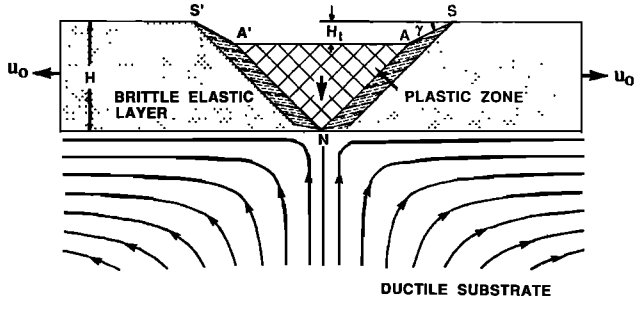

Fig. 8. A rift model in which the work required for lithospheric extension is minimized. In this rift there is only one plastic zone which forms the rift valley. The motion in the viscous substrate is induced by the horizontal separation of the lithospheric plates. The direction of viscous flow is shown by arrows on the stream lines.

The forces and bending moment acting on the elastic plate are calculated by directly integrating the stresses given in equations (15) along the edge of the elastic plate (line SANIJ in Figure 1):

$$F_x = \int_{SANIJ} \bar{\sigma}_x\, dy$$

$$= 2k(H-H_t-H_b) + (1/2)[\rho_1 g H_t^2 + (\rho_a-\rho_1)gH_b^2]$$

$$+ \rho_1 g H_t(H_N-H_t) + (\rho_a-\rho_1)gH_b(H-H_N-H_b) \quad (20a)$$

$$F_y = \int_{SANIJ} \bar{\sigma}_y\, dy$$

$$= (1/2)[\rho_1 g H_t^2 + (\rho_a-\rho_1)gH_b^2]$$

$$+ \rho_1 g H_t(H_N-H_t) + (\rho_a-\rho_1)gH_b(H-H_N-H_b) \quad (20b)$$

For a specific example with $H_N = H$ and $\rho_a = \rho_1$, the calculated forces F_x and F_y are plotted in Figure 9*a* as a function of the surface extension ΔL. We note that the required driving force F_x increases with the amount of extension. The increase in the required driving force is due to the deepening of the surface depression at the rift and the resulting horizontal forces created by the topography. This implies that a greater driving force is required to achieve a greater amount of extension. In this case quasi-static, stable rifting of brittle lithosphere occurs. If $H_N \neq H$, the required extensional force depends also on the density difference between the lithosphere and asthenosphere (Figure 9b). For a specified rift plastic zone geometry (a given H_N), smaller driving force is required to cause rifting in a lithosphere overlying a less dense asthenosphere ($\rho_a < \rho_1$).

Uplift of Rift Shoulders

The formation of a rift basin causes a mass deficit at rift zone and unloads the lithosphere. Since the lithospheric plates outside the rift zone have elastic strength, the lithosphere responses to the deepening rift basin by regional isostatic compensation: flanks of the rift shoulder deflect upward by elastic flexure, and the wavelength of the deflection is wider than the rift graben itself. The amount of elastic deflection can be calculated as a function of extension.

The calculated vertical force F_y increases as the rift basin deepens (Figure 9a). This vertical force causes uplift of rift shoulders so that the unloading due to rift basin formation can be isostatically compensated. We have also calculated the bending moment M_o , which can cause uplift of rift shoulders as well. When the thin elastic plate outside the

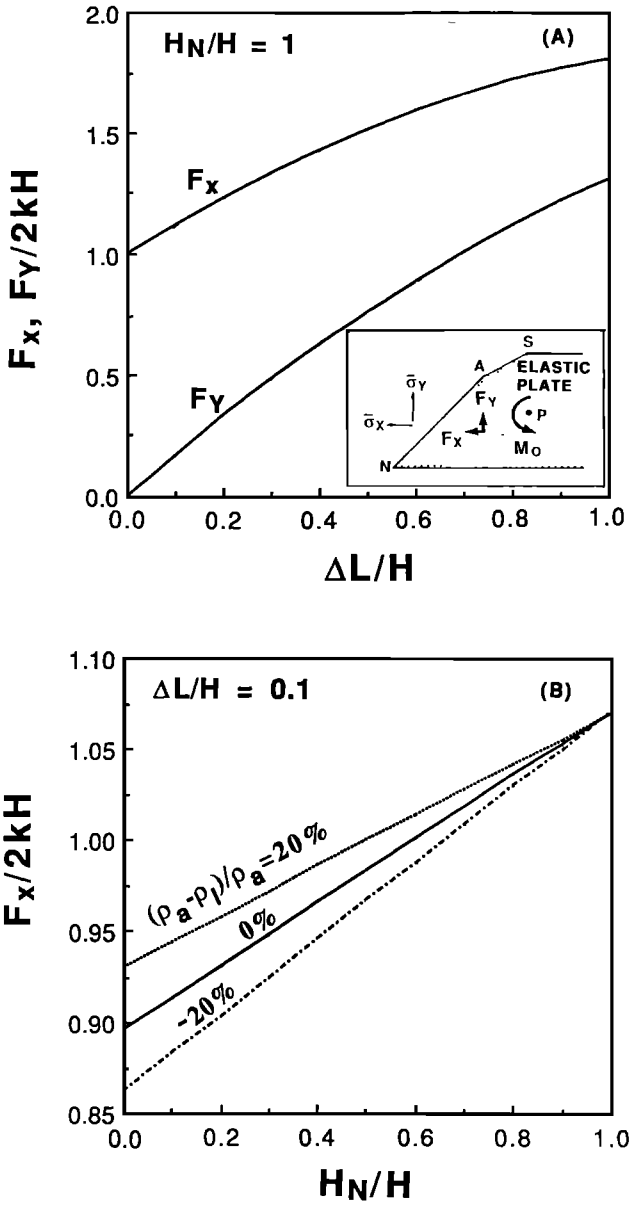

Fig. 9. (*a*) Inset illustrates the forces and bending moment acting on the elastic lithosphere, which are calculated by integrating deviatoric stresses along line SAN. Solid line shows the horizontal deviatoric force F_x as a function of total surface extension ΔL. Dashed line shows the vertical load F_y as a function of ΔL. This example is shown for $H_N = H$, $\rho_a = \rho_l = 3.0 \times 10^3$ Mg/m^3, $k = 40$ MPa. (*b*) Dependence of the required extensional force on rift geometry and the density difference between the lithosphere and asthenosphere . This example is shown for $\Delta L = 0.1$ H. When $H_N = H$, there is only an upper plastic zone. When $H_N = 0$, there is only a lower plastic zone. Note that for a given H_N, the required extensional force is smaller for smaller values of $\rho_a - \rho_l$.

rift plastic zone is subjected to a line load F_y and a bending moment M_o at x=0, position location of the rift shoulder, the equilibrium small deflection $\delta(x)$ can be evaluated based on thin plate bending equations [*Turcotte and Schubert*, 1982, p. 128]:

$$\delta(x) = l^2/(2D)\ \exp(-x/l)\ [-M_o \sin(x/l) + (F_y\, l + M_o)\cos(x/l)] \quad (21)$$

where $D = EH^3/[12(1-\upsilon^2)]$ is the flexural rigidity of the elastic plate, E is Young's modulus, and υ is Poisson's ratio. The flexure length of the elastic plate is $l = [4D/(\rho_l g)]^{1/4}$. For plausible values of E and υ (Table 1), the flexural length l of a 10-km-thick elastic plate (H = 10 km) is about 35 km.

Vening Meinesz [1950] predicted a rift valley width which is controlled by the flexural length of an elastic plate. For a 10-km-thick elastic plate with flexural length of 35 km, the predicted Vening Meinesz width of rift valley is about 28 km. In the present model, however, the initial width of the rift valley is proportional to the original thickness of the upper plastic zone H_N. For the minimum work solution in which $H_N = H$ (Figure 8), we predict a 20-km initial rift valley width when the brittle plate thickness H is 10 km. For other cases in which $H_N < H$, even narrower initial width of rift valley is expected.

The calculated deflection for different stages of rifting is superimposed on lithospheric stretching in Figure 10. It is found that every kilometer of plate thinning will create roughly 600 m of flank uplift. We also found that about 95% of rift shoulder uplift is due to the vertical force F_y and the effect of bending moment M_o can be neglected in calculating first-order elastic deflection of the brittle layer. This approximation has been made in simple models of *Vening Meinesz* [1950], *Heiskanen and Vening-Meinesz* [1958], and *Jackson and McKenzie* [1983].

Several authors have considered other two processes that modify the uplifted rift shoulders: (1) erosion of the rift shoulders and sedimentary filling of the rift basin [e.g., *King et al.*, 1988; *Stein et al.*, 1988], and (2) additional long-term subsidence or uplift due to reequilibrium of the thermally stratified lithosphere [e.g., *Salveson*, 1976, 1978; *McKenzie*, 1978; *Keen*, 1985, 1987; *Hellinger and Sclater*, 1983; *Steckler*, 1985; *Buck*, 1986]. In this paper we attempt to focus only on the fundamental characteristics of rifting in brittle lithosphere. The erosion and thermal processes have not been integrated into the present model. A more obvious consequence of erosion is the smoothing of rift topography due to the sedimentary filling of rift valley. Results of Figure 9a suggest that a rift with smoother topography (corresponding to smaller ΔL) requires smaller driving force F_x. It is plausible that continuous erosion might facilitate further development of a rift by reducing the required extensional force.

Purely mechanical models such as those examined in this paper describe rapid rifting in which the rate of lithospheric extension is much faster than that of thermal conduction, so that isotherms in the lithosphere move with the deforming material. In this case, the thickness of the undeformed lithosphere depends only on the initial thermal state of the lithosphere. On the other hand, if the rate of extension is slow, thermal conduction and advection could significantly alter the thickness of the brittle lithosphere during rifting [e.g., *England*, 1983; *Sawyer*, 1985]. Mid-ocean ridge rifts are examples of thermally controlled rifts, in which a steady state lithosphere thickness is maintained [e.g., *Phipps Morgan et al.*, 1987; *Lin and Parmentier*, 1989]. The width of mid-ocean ridge rifts often varies significantly along the axis of slow spreading ridges with wider rift valley observed in the vicinity of cold transforms [e.g., *Fox and Gallo*, 1984]. Since the width of a rift is proportional to the thickness of the brittle lithosphere, the wider rift valley

Table 1. Notation

Symbol	Quantity	Value Used	Units
σ_1	maximum compressive stres		Pa
σ_3	minimum compressive stres		Pa
σ_x	normal stress in the x-direction (horizontal)		Pa
σ_y	normal stress in the y-direction (vertical)		Pa
τ_{xy}	shear stress		Pa
$\bar{\sigma}_x, \bar{\sigma}_y, \bar{\tau}_{xy}$	stresses in excess of lithostatic overburden		Pa
k	von Mises failure coefficient	40	MPa
C_o	cohesive strength	0	Pa
σ_n	normal stress at top or bottom boundary		Pa
σ_s	shear stress at top or bottom boundary		Pa
p	average stress, equal to - $(\sigma_1 + \sigma_3)/2$		Pa
ϕ	angle of internal friction		o
θ	counterclockwise angle between x-direction and σ_3		o
u_x	velocity component in the x-direction		m s^{-1}
u_y	velocity component in the y-direction		m s^{-1}
u_α	velocity component along an α line		m s^{-1}
u_β	velocity component along a β line		m s^{-1}
F_x	horizontal force per unit length		N m^{-1}
F_y	vertical force per unit length		N m^{-1}
M_o	bending moment per unit length		N
δ	vertical deflection of elastic plate		m
γ	surface slope of deformed regions		o
x	horizontal coordinate		km
y	vertical coordinate		km
W_A	width of active rift (rift graben)		km
W_S	distance between rift shoulders		km
H	initial thickness of brittle layer		km
H_N	thickness of upper plastic zone		km
H_t	depth of rift valley		km
H_b	relief of plastic zone at bottom surface		km
ΔL	amount of lithospheric extension at surface		km
l	flexural length of elastic plate		km
ρ_1	density of brittle lithosphere		Mg m^{-3}
ρ_a	density of ductile substrate		Mg m^{-3}
g	acceleration of gravity	9.8	m s^{-2}
U	gravitational potential of plastic zones		J s^{-1} m^{-1}
E	rate of energy dissipation in resisting material shear strength		J s^{-1} m^{-1}
W	rate of work by external surface forces on plastic zones		J s^{-1} m^{-1}
E	Young's modulus	3.0×10^{10}	Pa
υ	Poisson's ratio	0.25	
D	flexural rgidity of elastic plate		N m
μ	viscosity of ductile substrate		Pa s

near transforms might simply indicate colder thus thicker lithosphere there.

Conclusions

To consider the role of faulting and brittle lithospheric deformation, we have formulated a model describing the formation of rifts as finite amplitude necking of an elastic-plastic layer overlying a fluid substrate. A perfectly plastic rheology is a continuum description of faulting. This model illustrates two important aspects of rift evolution that previous models do not treat explicitly: the evolution of the rift width as extension proceeds and the finite strain that occurs. A region at yield initially develops with a width determined by the thickness of the layer and the geometry of the bounding slip lines. As extension proceeds, the surface within the rift subsides, and the width of the subsiding yield zone decreases. At any stage of rifting, material in regions just outside the yield zone is deformed but no longer deforming. The width of these deformed regions increases with increasing extension. Vertical forces due to the mass deficit of the rift depression will flex the elastic layer outside the yield zone, creating flanking uplifts.

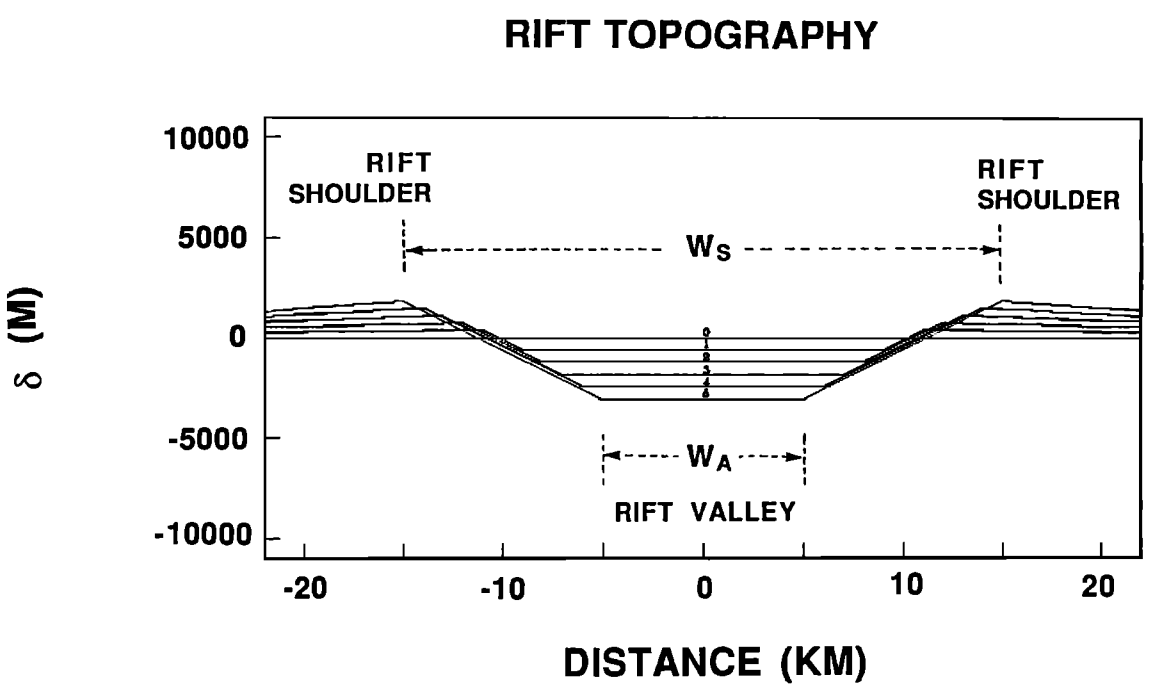

Fig. 10. Predicted successive rift topography in a 10-km-thick lithospheric plate. The model includes the subsidence of rift graben and uplift of rift shoulders by regional isostatic compensation. Note that as the rift basin deepens, the active rift valley W_A narrows, while the distance between rift shoulders W_S widens.

This model makes several important predictions for the morphology and structural evolution of rift zones. First, faulting should extend to the rift shoulders but not beyond, and the rift shoulders will widen as extension accumulates. However, the rift, defined as the region in which the surface is subsiding, narrows with increasing extension. Models in which necking is controlled by ductile flow predict that rifts should widen with increasing extension [e.g., *Keen*, 1985]. Field examples in rift zones show that the region of active faulting and subsidence narrows with increasing extension. This indicates the important role of deformation within a brittle lithospheric layer in controlling rift structure and evolution. Second, since the required extensional force increases with the amount of extension, lithospheric stretching in rift zones is a quasi-static, stable process. Finally, because the yield zone will revert to elastic behavior if the external force causing extension is removed, the model predicts that the rift depression and flanking uplifts will be preserved indefinitely after extension stops.

Appendix A: Calculation of Stress and Velocity Fields in Plastic Zone

Stress Field

The stress field in plastic zones is constructed in a piecewise fashion downward from the upper surface and upward from the lower surface of the plastic zones. As an example, we show how to construct stress and velocity fields for the upper plastic zone (area ABCNC'B'A'O in Figures 4*a* and 4*b*). The procedure for constructing the lower plastic zone is the same except that different stress boundary conditions (equation (8)), should be used instead.

Since the upper surface is a free surface, σ_n and σ_s are zero along AOA'. To convert these values into the variables σ and θ, we use the following expressions [*Sokolovskii*, 1965, p. 14]:

$$\sigma = p' \sin\Delta/\sin(\Delta-\delta') \quad \text{(A1)}$$

$$\theta = \lambda + \alpha \quad \text{(A2)}$$

where

$$p' = [(\sigma_n + C_n/\tan\phi)^2 + \sigma_s]^{1/2} \quad \text{(A3)}$$

$$\delta' = \tan^{-1}[\sigma_s/(\sigma_n + C_n/\tan\phi)] \quad \text{(A4)}$$

$$\Delta = \sin^{-1}(\sin\delta'/\sin\phi) \quad \text{(A5)}$$

$$\lambda = \pi/2 + 1/2(-\Delta-\delta') \quad \text{(A6)}$$

and α is the slope of the upper surface.

Starting from line AO, we can successively obtain stress fields for blocks ABO, BCO and CON according to following procedure.

Step 1 (block ABO). Suppose we are to calculate both the x-y position of point P and the stresses at P from the given positions and stresses of points 1 and 2 along line AO (Figure 4*a*). To get the x-y coordinates of point P, we apply the the first recurrence formula (with + sign) of equation (6*a*) along line 1P (α line) and the second formula (with negative sign) along line 2P (β line). The two sets of recurrence formula in equation (6*b*) are then applied along line 1P and 2P to determine the values of σ and θ at point P. From the known stresses along boundary AO, such procedure can be continued to obtain stress solutions at any point in block AOB.

Step 2 (block BOC). Due to a discontinuity in surface slope at point O, there is a stress singularity at the point O, for which a special formula for stress is needed [*Sokolovskii*, 1965, p. 26]:

$$\sigma = (1 + \sin\phi) \exp[(\pi-2\theta)\tan\phi] \quad \text{(A7)}$$

Approaching point O from boundary BO and boundary CO, the θ value change from $\pi/2-\alpha$ to $\pi/2$. Using the known stress conditions along boundary BO and formula (A1), we can construct the slip line field in block BOC.

Step 3 (block CON). Due to the symmetric requirement about the center line ON, θ is $\pi/2$ along boundary ON. This condition, together with the known stress values at OC, is sufficient for calculating stresses at all the points inside block CON. Readers are referred to *Sokolovskii* [1965, p. 117] for more details in numerical procedures.

Velocity Field

Once the slip line field is determined, the velocity field can be constructed in a similar piecewise fashion (Figure 4*b*). This time, however, we need to calculate velocity in the following order: first at block COC'N, second at blocks OBC and OC'B', and finally at blocks AOB and A'OB'. Horizontal velocity is equal to $+u_o$ along boundary ABCN and $-u_o$ along A'B'C'N'. Along both boundaries, the vertical velocity is zero. The finite-difference forms of recurrence equations (12*a*) and (12*b*) are used in velocity calculations.

Appendix B: Solutions of Stress and Velocity Fields in Viscous Substrate

In this section we derive the rate of work required to deform the viscous substrate underlying the brittle lithosphere. The mantle substrate is idealized as a viscous half-space with flat top surface. If no slip occurs at the interface between the brittle lithsosphere and the viscous subtrate, the velocities of the mantle substrate match those of the deforming brittle lithosphere at the interface. Considering a rift in which the base of the lower plastic zone is 2s wide, the required velocities at y = 0 are

$$u_x = -u_o,\ u_y = 0 \qquad \text{for } -\infty < x < -s \qquad \text{(B1}a\text{)}$$

$$u_x = 0,\ u_y = u_o \qquad \text{for } -s < x < +s \qquad \text{(B1}b\text{)}$$

$$u_x = u_o,\ u_y = 0 \qquad \text{for } +s < x < +\infty \qquad \text{(B1}c\text{)}$$

where u_x and u_y are the horizontal and vertical velocities and u_o is the horizontal velocity of the undeforming plates. For these boundary conditions, stress and velocity fields in the half-space can be determined uniquely by solving the equations on stress equilibrium and mass conservation [e.g., *Batchelor*, 1967].

We have obtained the stress and velocity solutions for this problem using the complex-variable techniques of *Muskhelishvili* [1953, p.584]. The stress field is given by

$$\frac{1}{2}(\sigma_{yy}-\sigma_{xx})+i\tau_{xy}= \left(\frac{\mu u_o}{\pi}\right)\left[\frac{(z+\bar{z})+i(-z+\bar{z})+2s}{(z+s)^2}+\frac{(z+\bar{z})+i(z-\bar{z})-2s}{(z-s)^2}\right] \qquad \text{(B2)}$$

and

$$\frac{1}{2}(\sigma_{xx}+\sigma_{yy}) = 2\,\mathrm{Re}\left\{\left(\frac{\mu u_o}{\pi}\right)\left[\frac{(1-i)}{z+s}+\frac{(1+i)}{-z+s}\right]\right\} \qquad \text{(B3)}$$

where μ is the mantle viscosity, $z = x + iy$ and $\bar{z} = x - iy$ are complex variables. The velocity field is given by

$$u_x + iu_y = \left(\frac{u_o}{2\pi}\right)\left[-iA+i\bar{A}-B-\bar{B}+iC-i\bar{C}+(z-\bar{z})\left(\frac{-1+i}{z+s}+\frac{-1-i}{z-s}\right)\right] \qquad \text{(B4}a\text{)}$$

where

$$A = \ln(t-z)\Big|_{t\to -\infty}^{t=-s} \qquad \text{(B4}b\text{)}$$

$$B = \ln(t-z)\Big|_{t=-s}^{t=+s} \qquad \text{(B4}c\text{)}$$

$$C = \ln(t-z)\Big|_{t=+s}^{t\to +\infty} \qquad \text{(B4}d\text{)}$$

The rate of energy dissipation in resisting the viscous motion of the substrate is

$$dE_{viscous}/dt = \int_{-\infty}^{\infty}\sigma_{yy}u_y\,dx + \int_{-\infty}^{\infty}\tau_{xy}u_x\,dx \qquad \text{(B5}a\text{)}$$

where the first term on the right-hand side, the energy dissipation due to the work of the vertical normal stress, is given by

$$\int_{-\infty}^{\infty}\sigma_{yy}u_y\,dx = \left(\frac{4\mu u_o^2}{\pi}\right)\left[-\ln(t)\Big|_{t\to 0}+\ln(2s)\right] \qquad \text{(B5}b\text{)}$$

and the second term, the energy dissipation due to the shear stress, is given by

$$\int_{-\infty}^{\infty}\tau_{xy}u_x\,dx = \left(\frac{4\mu u_o^2}{\pi}\right)\left[2\ln(t)\Big|_{t\to\infty}-\ln(t)\Big|_{t\to 0}-\ln(2s)\right] \qquad \text{(B5}c\text{)}$$

Substituting Equations (B5*b*) and (B5*c*) into (B5*a*), we arrive at

$$dE_{viscous}/dt = \left(\frac{8\mu u_o^2}{\pi}\right)\left[\ln(t)\Big|_{t\to\infty}-\ln(t)\Big|_{t\to 0}\right] \qquad \text{(B5}d\text{)}$$

We note that the right-hand side of equation (B5*d*) is not a function of the plastic zone width s. This implies that the total rate of energy dissipation of the viscous flow is the same for different sizes of the lower plastic zone.

Acknowledgments. We thank David Sparks, Jason Phipps Morgan, Robert Detrick, Tim Byrne, and Paul Hess for comments on the manuscript and Ross Stein and Geoffrey King for furnishing preprints of their papers. W. Jason Morgan, Roger Buck, and Yongshun John Chen provided thorough reviews of the manuscript. Ms. Mona Delgado typeset the manuscript. This research was supported by NASA grant NSG 7605 and supplemented by the WHOI Culpeper Young Scientist Award (J.L.) from the Culpeper Foundation. Wood Hole Oceanographic Institution contribution 7151.

References

Artemjev, M.E., and E.V. Artyushkov, Structure and isostasy of the Baikal Rift and the mechanism of rifting, *J. Geophys. Res., 76*, 1197-1211, 1971.

Batchelor, G.K., *An Introduction to Fluid Dynamics*, 615 pp., Cambridge University Press, New York, 1967.

Bott, M.H.P., Formation of sedimentary basins of graben type by extension of the continental crust, *Tectonophysics, 36*, 77-86, 1976.

Bott, M.H.P., and D.P. Mithen, Mechanisms of graben formation- the wedge subsidence hypothesis, *Tectonophysics, 94*, 11-22, 1983.

Brace, W.F., and D.L. Kohlstedt, Limits on lithosphere stress imposed by laboratory experiments, *J. Geophys. Res., 85*, 6248-6252, 1980.

Buck, W.R., Small-scale convection induced by passive rifting: The cause for uplift of rift shoulders, *Earth Planet. Sci. Lett., 77*, 362-372, 1986.

Burke, K., Evolution of continental systems in light of plate tectonics in *Tectonics and Geophysics of Continental Rifts*, edited by I. B. Ramberg, and E.R. Neumann, pp. 1-9, Dordrecht, Reidel, 1978.

Byerlee, J.D., Brittle-ductile transition in rocks, *J. Geophys. Res., 73*, 4741-4750, 1968.

Chapple, W.M., Mechanics of thin-skined fold-and-thrust belts, *Geol. Soc. Am. Bull., 89*, 1189-1198, 1978.

Cloos, E., Experimental analysis of gulf coast fracture patterns, *Am. Assoc. Petr. Geol. Bull., 52*, 420-444, 1968.

Cochran, J.R., Effects of finite extension times on the development of sedimentary basins, *Earth Planet. Sci. Lett., 66*, 289-302, 1983.

Davis, D., J. Suppe, and F.A. Dahlen, Mechanics of fold-and thrust belts and accretionary wedges, *J. Geophys. Res., 88*, 1153-1172, 1983.

Easton, R.M., Crustal structure of rifted continental margins: Geological constraints from the Proterozoic rock of the Canadian Shield, *Tectonophysics, 94*, 371-390, 1983.

Ebinger, C.J., M.J. Crow, B.R. Rosendahl, D.A. Livingstone, and J. LeFournier, Structural evolution of Lake Malawi, Africa, *Nature, 308*, 627-629, 1984.

Ebinger, C.J., B.R. Rosendahl, and D.J. Reynolds, Tectonic model of the Malawi rift, Africa, *Tectonophysics, 141*, 215-235, 1987.

Elliott, D., The motion of thrust sheets, *J. Geophys. Res., 81*, 949-963, 1976.

England, P., Constraints on extension of continental lithosphere, *J. Geophys. Res., 88*, 1145-1152, 1983.

Fox, P.J., and D.G. Gallo, A tectonic model for ridge-transform-ridge plate boundaries: Implications for the structure of oceanic lithosphere, *Tectonophysics, 104*, 205-242, 1984.

Gibbs, A.D., Structural evolution of extensional basin margins, *J. Geol. Soc. Lond., 141*, 609-620, 1984.

Goetze, C., and B. Evans, Stress and temperature in the bending lithosphere as constrained by experimental rock mechanics, *Geophys. J. R. Astron. Soc., 59*, 463-478, 1979.

Hafner, W., Stress distributions and faulting, *Geol. Soc. Am. Bull., 62*, 373-398, 1951.

Heiskanen, W.A., and F.A. Vening-Meinesz, *The Earth and Its Gravity Field*, 470 pp., McGraw-Hill, New York, 1958.

Hellinger, S.J., and J.G. Sclater, Some comments on two-layer extensional models for the evolution of sedimentary basins, *J. Geophys. Res., 88*, 8251-8269, 1983.

Hill, R., *The Mathematical Theory of Plasticity*, 356 pp., Clarendon Press, Oxford, 1950.

Horsfield, W.T., Contemporaneous movement along crossing conjugate normal faults, *J. Struct. Geol., 2*, 305-310, 1980.

Illies, J.H., The Rhine graben rift system - Plate tectonics and transform faulting, *Geophys. Surv., 1*, 27-60, 1972.

Jackson, J.A., and D. McKenzie, The geometrical evolution of normal fault systems, *J. Struct. Geol, 5*, 471-482, 1983.

Keen, C.E., The dynamics of rifting: Deformation of the lithosphere by active and passive driving forces, *Geophys. J. R. Astron. Soc., 80*, 95-120, 1985.

Keen, C.E., Dynamical extension of the lithosphere during rifting: Some numerical model results in *Composition, Structure and Dynamics of the Lithosphere-Asthenosphere System, Geodyn. Ser.*, vol. 16, edited by K. Fachs and C. Froidevaux, pp. 189-203, AGU, Washington, D.C., 1987.

King, G.C.P., R.S. Stein, and J.B. Rundle, The growth of geological structures by repeated earthquakes, 1, Conceptual framework, *J. Geophys. Res., 93*, 13,307-13,318, 1988.

Kirby, S.H., Rheology of the lithosphere, *Rev. Geophys., 21*, 1458-1487, 1983.

Kligfield, R., J. Crespi, S. Naruk, and G.I.H. Davis, Displacement and strain patterns of extensional orogens, *Tectonics, 3*, 577-609, 1984.

Lin, J., and E.M. Parmentier, Mechanisms of lithospheric extension at mid-ocean ridges, *Geophys. J., 96*, 1-22, 1989.

McKenzie, D., Some remarks on the development of sedimentary basins, *Earth Planet. Sci. Lett., 40*, 25-32, 1978.

Muskhelishvili, N.I., *Some Basic Problems of the Mathematical Theory of Elasticity*, 704 pp., Nordhoff, Leyden, Netherlands, 1953.

Parmentier, E.M., Dynamic topography in rift zones: Implications for lithospheric heating, *Philos. Trans. R. Soc. London, Ser. A, 321*, 23-25, 1987.

Parmentier, E.M., E.R. Stofan, and J.W. Head, A finite amplitude necking model for the formation and evolution of rift zones: Application to the Beta Regio rift (abstract), *Lunar Planet. Sci., XVIII*, 764-765, 1987.

Phipps Morgan, J., E.M. Parmentier, and J. Lin, Mechanisms for the origin of mid-ocean ridge axial topography: Implications for the thermal and mechanical structure of accreting plate boundaries, *J. Geophys. Res., 92*, 12,823-12,836, 1987.

Ramberg, I.B., and P. Morgan, Physical characteristics and evolutionary trends of continental rifts, *Proceedings of the 27th Geological Congress, 7*, 165-216, 1984.

Ramberg, I.B., and E.R. Neumann (Eds.), *Tectonics and Geophysics of Continental Rifts*, D. Reidel, Hingham, Mass.,1978.

Rosendahl, B.R., Architecture of continental rifts with special reference to East Africa, *Annu. Rev. Earth Planet. Sci., 15*, 445-503, 1987.

Royden, L., and C. E. Keen, Rifting processes and thermal evolution of the continental margin of eastern Canada

determined from subsidence curves, *Earth Planet. Sci. Lett., 51,* 343-361, 1980.

Rundle, J.B., Viscoelastic-gravitational deformation by a rectangular thrust fault in a layered earth, *J. Geophys. Res., 87,* 7787-7796, 1982.

Salencon, J., *Applications of the Theory of Plasticity in Soil Mechanics,* 158 pp., John Wiley, New York, 1974.

Salveson, J.O., Variations in the oil and gas geology of rift basins, paper presented at Fifth Exploration Seminar, Egypt. Gen. Petr. Corp., Cairo, Egypt, Nov. 15-17, 1976.

Salveson, J.O., Variations in the geology of rift basins-A tectonic model, paper presented at Rio Grande Rift Symposium, Santa Fe, N. M., Oct. 1978.

Savage, J.C., and G. Gu, A plate flexure approximation to postseismic and interseismic deformation, *J. Geophys. Res., 90,* 8570-8580, 1985.

Sawyer, D.S., Brittle failure in the upper mantle during extension of continental lithosphere, *J. Geophys. Res., 90,* 3021-3025, 1985.

Shudofsky, G. N., Source mechanisms and focal depths of East African earthquakes using Rayleigh-wave inversion and body-wave modelling, *Geophys. J. R. Astron. Soc., 83,* 563-614, 1985.

Sokolovskii, V.V., *Statics of Granular Media,* 270 pp., Pergamon, New York, 1965.

Steckler, M. S., Uplift and extension at the Gulf of Suez: Indications of induced mantle convection, *Nature, 317,* 135-139, 1985.

Steckler, M. S., and A.B. Watts, Subsidence history and tectonic evolution of Atlantic-type continental margins, *in Dynamics of Passive Margins, Geodyn. Ser.,*vol. 6, edited by R. A. Scrutton, pp.184-196, AGU, Washington, D.C., 1982.

Stein, R.S., G.C.P. King, and J. B. Rundle, The growth of geological structures by repeated earthquakes, 2, Field examples of continental dip-slip faults, *J. Geophys. Res., 93,* 13,319-13,331, 1988.

Turcotte, D.L., and G. Schubert, *Geodynamics,* 450 pp., John Wiley, New York, 1982.

Vening Meinesz, F. A., Les "graben" africains resultat de compression ou de tension dans la croute terrestre, *Inst. R. Colon. Belge Bull. Seances, 21,* 539-552, 1950.

Villemin, T., F. Alvarez, and J. Angelier, The Rhinegraben: Extension, subsidence and shoulder uplift, *Tectonophysics, 128,* 47-59, 1986.

Zorin, Y.A., and V.A. Rogozhina, Mechanism of rifting and some features of the deep-seated structures of the Baikal rift zone, *Tectonophysics, 45,* 23-30, 1978.

Zuber, M.T., and E.M. Parmentier, Lithospheric necking: A dynamic model for rift morphology, *Earth Planet. Sci. Lett., 7,* 373-383, 1986.

J. Lin, Department of Geology and Geophysics, Woods Hole Oceanographic Institution, Woods Hole, MA 02543.

E.M. Parmentier, Department of Geological Sciences, Brown University, Providence, RI 02912.

(Received May 5, 1989;
revised September 22, 1989;
accepted September 23, 1989.)